SPE/Petroleum Society of CIM/CHOA 79028

Injection pressures for geomechanical enhancement of recovery processes in the Athabasca oil sands

Patrick M. Collins, SPE/CIM/CHOA, Petroleum Geomechanics Inc.

This paper was prepared for presentation at the SPE International Thermal Operations and Heavy Oil Symposium and International Horizontal Well Technology Conference held in Calgary, Alberta, Canada, 4–7 November 2002.

Abstract

This paper describes a geomechanical approach to the determination of injection pressures that will result in formation shearing within the Athabasca oil sands. The enhancement of *in situ* permeabilities, resulting from shearing, is a beneficial phenomenon and often an essential prerequisite of many successful *in situ* recovery processes.

This geomechanical analysis is based upon the general geological setting in the Athabasca oil sands, observations made from field data, published laboratory data, and geomechanical principles. The first objective was to estimate the existing stress state in the rock. This determination was based on elastic theory and tectonics, and fitted to field measurements of the minimum *in situ* stress from minifrac tests in the Athabasca oil sands. The methodology also calculates the maximum horizontal stress, a parameter that is extremely difficult to measure, yet is an important parameter for most stress analyses. The resultant stress anisotropy creates the potential for formation shearing; a potential that is unleashed once the effective stresses are sufficiently reduced with high injection pressures.

Lastly, the amounts by which injection pressures must be increased for shear failure are provided, assuming typical values of formation strength.

The analysis begins with a determination of the minimum *in situ* stress, as a function of depth. This is the fracture closure pressure that is a useful parameter in determining fracture treatment pressures, fracture containment, and fracture orientation. The associated tectonic strain is used to calculate the maximum horizontal stress. Using the maximum and minimum stresses, the injection pressure at which extensive shearing will occur is calculated. This is the geomechanical optimum operating pressure. While other considerations may favour a lower operating pressure, recovery processes that rely upon high *in situ* permeabilities may not be viable at lower injection pressures.

The methodology presented is applicable to other regions.

Introduction

A large number of *in situ* recovery processes in the Athabasca region involve the injection of fluids into oilsands in order to mobilize the highly viscous bitumen resource. Typically, injection pressures are selected on the basis of a large number of numerical simulations of the process, using conventional reservoir parameters and conventional reservoir simulators. Unfortunately, these typically exclude any geomechanical effects, since any bulk volume change in the reservoir gridblocks is rarely an allowable option. This is despite field evidence of significant movements, both laterally and vertically, confirming reservoirs can dilate in response to the fluid injection.

Past optimization of injection pressures has focussed heavily on thermodynamic efficiencies. While thermodynamic efficiency is commendable, other significant and dominant effects must also be considered. Geomechanical enhancement of the reservoir permeability, porosity, and fluid mobility is one major effect, without which, the goal of thermodynamic efficiency may not be effective.

This paper presents a simple, logical methodology to determine the minimum injection pressure at which full geomechanical effects will be attained. While geomechanics have an effect at lower pressures, the optimal geomechanical injection pressure will be such that shear failure occurs within the formation.

Determination of Horizontal Stress

The basic premise for the determination of stresses in rock is that the rock can be described by Hooke's Law[1] for the range of applicable stresses:

$$\varepsilon_x E = \sigma_x - \upsilon(\sigma_y + \sigma_z) \quad \text{.....[1]}$$

$$\varepsilon_y E = \sigma_y - \upsilon(\sigma_x + \sigma_z) \quad \text{.....[2]}$$

$$\varepsilon_z E = \sigma_z - \upsilon(\sigma_x + \sigma_y) \quad \text{.....[3]}$$

and the principle of effective stress (Terzaghi, 1943)[2]:

$$\sigma' = \sigma - p_f \quad \text{.....[4]}$$

where

ε_x , ε_y , ε_z are the principal strains

σ_x , σ_y , σ_z are the principal stresses

E is Young's modulus

ν is Poisson's ratio

σ is the total stress

σ' is the effective stress (i.e., carried by the solid matrix)

p_f is the formation fluid pressure

The Terzaghi effective stress equation assumes that only the pore pressure resists any increase in applied confining pressure. If the pore fluid compressibility is high, relative to the rock matrix compressibility, then the pressure term must be modified[3]:

$$\Delta\sigma' = \Delta\sigma - \alpha\Delta p_f \quad \text{.....[5]}$$

$$\alpha = 1 - \frac{K}{K_s'} \quad \text{.....[6]}$$

where

α is the Biot-Willis coefficient of pore pressure

K is the bulk modulus with constant pore pressure (i.e., drained condition; therefore, the matrix modulus)

K_s' is the unjacketted bulk modulus (i.e., the average solid grain modulus)

The Biot-Willis "α" is a measure of the efficiency with which the internal pore pressure resists any increase in confining pressure while undergoing volumetric strain under undrained conditions.[3] As such, it varies from 0 to 1 for perfectly compressible to incompressible fluids, respectively. Note that Equation 5 is applicable to a *change* in pore pressure from an initial value.

Horizontal Stress assuming Zero Lateral Strain. The equation for horizontal stress in an poroelastic medium, assuming no lateral strain, was given by Eaton (1969)[4] as:

$$\sigma_h = \frac{\upsilon}{1-\upsilon}\left(\sigma_v - p_f\right) + p_f \quad \text{.....[7]}$$

where

σ_h is the horizontal stress (a uniform stress)

σ_v is the vertical stress

This Eaton equation is valid for a quiescent depositional basin, in which no horizontal strains occur, and no change in formation fluid pressure has occurred. The horizontal stress is the rock's resistance to Poisson's lateral expansion in response to the net weight of the overburden (i.e., effective stress), plus the formation fluid pressure component.

Generalized Equation for Horizontal Stress. Rarely are the horizontal stress magnitudes exactly described by Eaton's equation. Even in tectonically inactive depositional environments, the process of sediment compaction usually results in lateral elongation of the beds. In addition, other factors alter the state of stress in the rock, resulting in horizontal stresses that can be higher or lower than those predicted by Eaton's equation. Usually, the horizontal stress becomes anisotropic, with the two principal horizontal stresses known as σ_{Hmax} and σ_{Hmin}.

Factors that modify the horizontal stresses from those predicted with Eaton's equation include changes in formation fluid pressure, tectonic strains, bed deformations, thermal change, and other effects (e.g.: diagenesis):

$$\sigma_h \Rightarrow \sigma_h + \Delta\sigma_{Pressure} + \Delta\sigma_{Tectonic} + \Delta\sigma_{Flexural} + \Delta\sigma_{Thermal} + \Delta\sigma_{Other} \quad \text{.....[8]}$$

Details are provided in the Appendices.

In situ Stresses in the Athabasca Oilsands

The usual assumption is that the three principal *in situ* rock stresses are the vertical stress and two orthogonal horizontal stresses. This is reasonable assumption for the Athabasca region. However, in areas of extensive geological deformation (e.g.: severe faulting, uplift, salt diapirism) the principal stress orientations may be tilted.

Horizontal Stress Anisotropy. Rarely, if ever, is the horizontal stress uniform. This is despite the fact that this is the starting assumption in most rock stress analyses. In many applications, such as hydraulic fracture stimulations, assuming uniform horizontal stress conditions often approximates the mimimum horizontal stress magnitude. At the same time, practitioners implicitly recognize stress anisotropy when analyses are done to determine the orientation of the maximum horizontal stress, and therefore of the induced fracture.

Stress Orientation. One of the most reliable means of determining the principal horizontal stress orientations is with borehole breakout analyses of vertical wells[5]. Calliper readings are normally recorded when running logs, therefore almost all wells have calliper data over the entire well length. Data from older wells are usually available. It is the volume of data over the length of each well, over a large number of wells, that provides overwhelming evidence for stress orientations.

Cox (1983)[6] noted the correlation between the breakout and stress orientations. In particular, he noted the NE-SW trend of the maximum horizontal stress throughout North America, east of the Rocky Mountains. **Figure 1** shows an outline of the Province of Alberta[7], with the Athabasca oil sands located in the northeast[8].

The schematic on the right shows the breakout orientation perpendicular to σ_{Hmax}. On this map, the orientation of the maximum horizontal stress, σ_{Hmax}, is determined predominantly with borehole breakout orientations. The highly consistent NE-SW trend, over a large number of wells

and over the entire province, is normally associated with a high horizontal stress anisotropy.

Figure 1 Maximum Horizontal Stress Orientations in Alberta

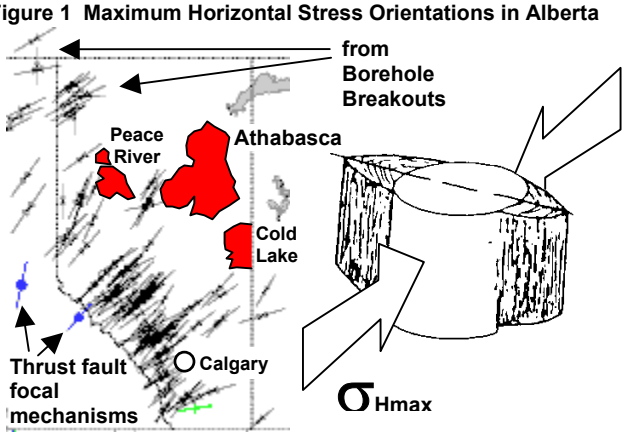

Stress Magnitudes.

Vertical Stress. The vertical stress is obtained by integrating the bulk density log. Alternatively, a gradient of 22 kPa/m or 1 psi/ft is a fair approximation of onshore densities. Most geomechanics analyses are insensitive to the slight variations from this value.

Pore Pressure. Pore pressure data is widely available for reservoir intervals, and less commonly available for the overburden. In the Athabasca, pressure monitoring instrumentation is often installed along horizontal SAGD wells, for control of wellbore hydraulics. Piezometers are usually installed in concert with thermocouples in observation wells. These will monitor the recovery process, and confirm that that process is contained so that there is no fluid communication with strata outside the reservoir. Geomechanics analyses are highly sensitive to the pore pressure.

Minimum In situ Stress. The magnitude of the minimum *in situ* stress is often a critical parameter to determine. Induced hydraulic fractures, both intentional and accidental, are propagated at or near this pressure, therefore it is often the maximum injection pressure for processes that are harmed by fracturing, or the minimum injection pressure for processes that require fracturing.

Uniform Horizontal Stress. A stress profile, assuming a uniform horizontal stress, can be approximated by applying Eaton's equation (Equation 7) to profiles of pore pressure, bulk density, and a derived Poisson's ratio from the dual sonic log. Laboratory-determined Poisson's ratios can be used in a similar manner to calculate the stress at the specimens' depths. Minifrac and hydraulic fracture stimulation values of the closure stress should be plotted as well, as these provide the best measurement of the minimum *in situ* stress.

The limitation of this approach is that it assumes zero lateral strain. While this is a reasonable assumption for younger depositional basins, it is simplistic for Alberta where the borehole breakout data display definite horizontal stress anisotropy, and are indicative of high anisotropy.

Tectonic Strain. A more reasonable assumption for stress magnitudes in the Athabasca oilsands is to assume that the uniform horizontal stresses have been modified by a subsequent tectonic strain. Given the unconsolidated structure of oil sands, core methods for the determination of stress magnitudes are inappropriate. Instead, the magnitude of *in situ* stresses can be estimated by arbitrarily applying a horizontal strain in one direction until the calculated minimum horizontal stress matches field data. The strain can then be used to calculate the maximum horizontal stress.

Figure 2 shows the effect of a uniaxial horizontal strain in the x-direction, assuming a typical[9] Athabasca oilsands Young's modulus and Poisson's ratio of (E,ν)=(800 MPa, 0.30). Constant gradients were assumed for the vertical stress and the pore pressure, although the pore pressure was shifted by 850 kPa to match field measurements.

Figure 2 Tectonic Stresses Resulting from A Uniaxial Horizontal Strain

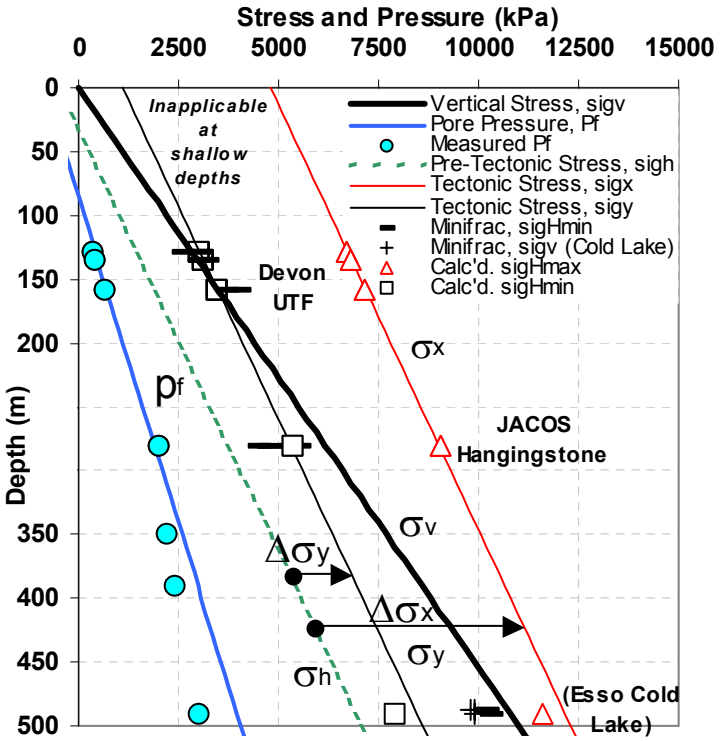

A profile of the pre-tectonic horizontal stress, labelled "sigh" or "σ_h", was calculated with Eaton's equation, assuming zero lateral strain. Minifrac data were available from the Devon UTF and JACOS Hangingstone projects that provided the minimum *in situ* stress[10,11]. Simulating tectonics, the lateral strain in the x-direction was increased until the minimum horizontal stress, in the y-direction, ("σ_y") intersected the minifrac data. This strain of ε_x =0.006 was then used to calculate the maximum horizontal stress, σ_x. The incremental tectonic stresses are labelled $\Delta\sigma_x$ and $\Delta\sigma_y$. Site-specific values of stress were calculated for both projects. These used the same assumptions, but used the measured pore pressures at each project.

The Esso Cold Lake project, outside of the Athabasca region, was added for comparison. Cold Lake oilsands are generally weaker, less stiff, and have higher Poisson's ratios under identical laboratory conditions. Therefore, the stress regime would differ slightly from the Athabasca region for the same applied strain. Cold Lake minifrac data[12] were interpreted to obtain values for the minimum horizontal stress and the vertical stress. Notably, the minimum horizontal stress was thought to be slightly larger than the vertical stress, in contrast to the Athabasca trend at that depth. This may be as a result of Cold Lake oilsands' higher Poisson's ratios.

Similarly, the minimum horizontal stress was slightly greater than the vertical stress at the Devon UTF project[10]. The fact that $\sigma_{Hmax} > \sigma_{Hmin} > \sigma_v$ is consistent with the hypothesis that the Athabasca region is tectonically affected.

Shear Failure. When rock is subjected to high differential compressive stresses, it fails in shear. For a frictional material such as oilsands, the strength is controlled by the internal friction angle of the rock. Once the ratio of the maximum and minimum effective stresses reaches a critical maximum, the rock fails.

Figure 3 Mohr-Coulomb Plot of the Injection Pressure Increase to Achieve Shear Failure

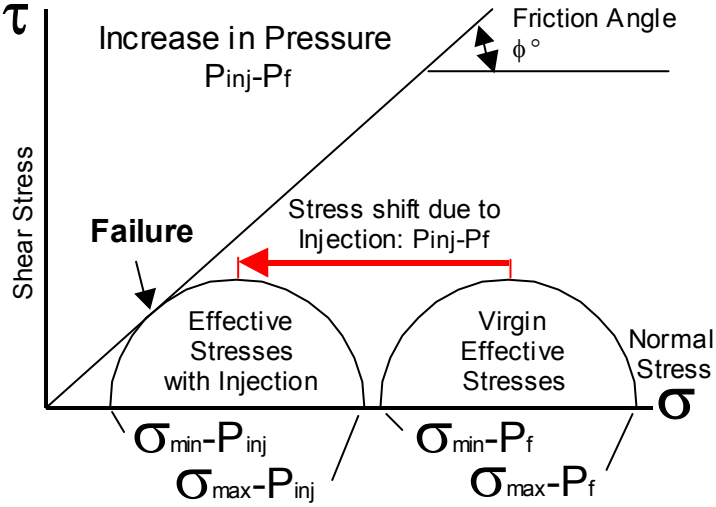

This is shown in the Mohr-Coulomb diagram (**Figure 3**) in which the stress state is plotted on axes of normal stress versus shear stress. The semi-circle on the right represents the Terzaghi effective stresses in the reservoir. The maximum and minimum stresses would be the two horizontal stresses, except at shallow depths where the vertical stress is the minimum stress.

The semi-circle on the left represents the same stress state, with all effective stresses reduced by the increase in formation pressure due to injection. The injection pressure, P_{inj}, is high enough to shift the Mohr Circle left until it intersects the frictional failure envelope, determined by the friction angle, $\phi°$. The stronger the rock, the higher the friction angle, and the higher the injection pressure has to be to ensure that the rock fails in shear.

Permeability and Porosity Enhancement due to Shear Failure. It is necessary to shear oilsands for most *in situ* recovery processes. The *in situ* permeabilities, although high in comparison to conventional reservoirs, will increase as the oilsands are subjected to shear stress. Shearing results in the permanent displacement and rotation of the constituent sand grains. This creates additional porosity, and enhances the "absolute" permeability. In oilsands, permeability is not an absolute, as it is highly dependent upon the degree of disturbance, which is quantified by the volumetric strain, i.e. porosity or dilation. Permeabilities can be increased by almost an order of magnitude if the oilsands fail in shear.

Figure 4 shows the significant effect of volumetric strain on the enhancement of absolute permeability in oilsands. These specimens were cored from block samples sawn from an outcrop of the McMurray Formation oilsands[13,14], in a region that had never been invaded by hydrocarbons. As such, it was bitumen-free and not subject to gas ex-solution and core disturbance problems associated with bitumen-rich core obtained by drilling and coring[15].

The graph on the left shows the results of triaxial tests on vertical specimens. Triaxial tests are usually conducted with a confining stress applied to the specimen, raising the axial stress until the specimen fails. These specimens dilate during the test as the individual grains rotate and displace, resulting in enhanced absolute permeability. At a volumetric strain of 5%, this increase is about 250%; at 10% volumetric strain, it is 600%. In the graph on the right, similar behaviour is seen for the horizontal specimens, with an enhancement of 160% at a 5% volumetric strain. Notably, the analytical predictions, such as the Kozeny-Carmen relationship, underestimate the permeability enhancement.

Figure 4 Absolute Permeability Increase with Dilation for Vertical and Horizontal Core, McMurray Formation Oilsands

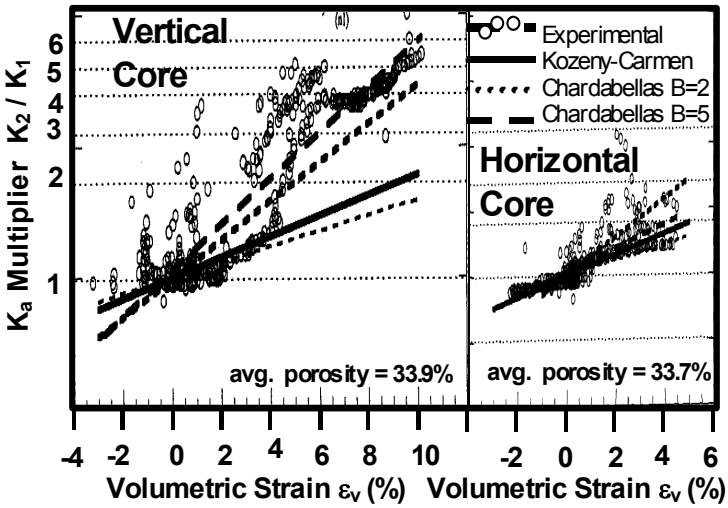

modified after Touhidi-Baghini (1998)

It should be emphasized that permeability data on quality oilsands specimens is extremely rare. Most oilsands core arrives in the physical-chemical laboratories with considerable disturbance already having occurred, and further disturbance

occurs during sampling and testing. Conventionally, absolute permeabilities of 10 Darcy are common, which is indicative of high core disturbance. These high-quality McMurray Formation specimens (**Figure 4**) began with permeabilities in the order of 1 to 2 Darcy, and achieved comparable enhanced permeabilities only after dilating.

Injection Pressures for Shear Failure. Shearing of the formation will result in dilation, and with it, an increase in porosity, absolute permeability, water saturation, and total fluid mobility. These are beneficial to *in situ* recovery schemes. While some dilation occurs at stress levels below failure, dilation its associated benefits are assured when the oilsands undergo shear failure.

Shear failure can be induced by increasing the stress differences, or by reducing the effective stresses until the oilsands fail. Reducing the effective stresses is achieved by increasing the injection pressure (**Figure 3**). This pressure can be calculated, knowing the existing rock stresses and assuming reasonable values for the rock strength.

Figure 5 shows the injection pressures required for shear failure in the Athabasca oilsands, as a function of friction angle. The tectonic rock stresses and the vertical stress are from Figure 2. The maximum stress is the horizontal stress in the x-direction.

The minimum stress is the vertical stress at shallow depths (< ~150m), and switches to the horizontal stress in the y-direction below 150m. This has implications for the development of shear planes: at shallow depths, the shear planes will be inclined ±25°-30° to the horizontal, whereas deeper, the shear planes will be vertical and oriented ±25°-30° to the direction of the maximum horizontal stress, i.e. NE-SW ±25°-30°. Recovery processes would be expected to preferentially expand laterally at shallow depths, and vertically when deeper. Geological heterogeneity, which can introduce oriented features of varying frictional resistance, will modify this behaviour.

Figure 5 includes predictions of injection pressures needed to initiate shear failure, for rock with friction angles of 20° to 60°. Friction angles of 20° to 30° are typical for weaker rocks such as mudstones and siltstones, and undisturbed sandstones have friction angles exceeding 50°.

The 2700 kPa injection pressure, P_{inj}, for the Devon UTF SAGD project (formerly AOSTRA UTF) is plotted, and it is approximately the injection pressure required to cause shear failure in an oilsand with a 50° friction angle. Similarly, the P_{inj} of 5000 kPa for the JACOS Hangingstone SAGD project is plotted. This high injection pressure was recognized as necessary to attain feasible steam chamber growth rates[11], and these were pre-determined with a series of minifracs in order to determine the local fracture stress of 4500-5300 kPa. The reported behaviour of both reservoirs in response to the SAGD process[9,11] was consistent with shearing within the reservoir.

Injection pressures for **Figure 5** were determined using the Mohr-Coulomb relationship, assuming no cohesion, and Terzaghi effective stress:

$$\sigma'_3 = \frac{\sigma_{max} - \sigma_{min}}{2} \frac{1 - \sin(\phi°)}{\sin(\phi°)} \quad \text{.....[9]}$$

$$P_{inj} = (\sigma_{min} - p_f) - \sigma'_3 \quad \text{.....[10]}$$

for a friction angle of $\phi° = 50°$,

$$P_{inj} = 15.0376(kPa/m) \cdot z(m) + 533(kPa) \quad \text{.....[11]}$$

where

σ_{max} is the maximum *in situ* stress
σ_{min} is the minimum *in situ* stress
σ'_3 is the effective confining stress at shear failure
P_{inj} is the injection pressure to achieve shear failure
z is the vertical depth (metres)

Figure 5 Injection Pressures for the Athabasca Oilsands as a Function of Shear Friction Angle

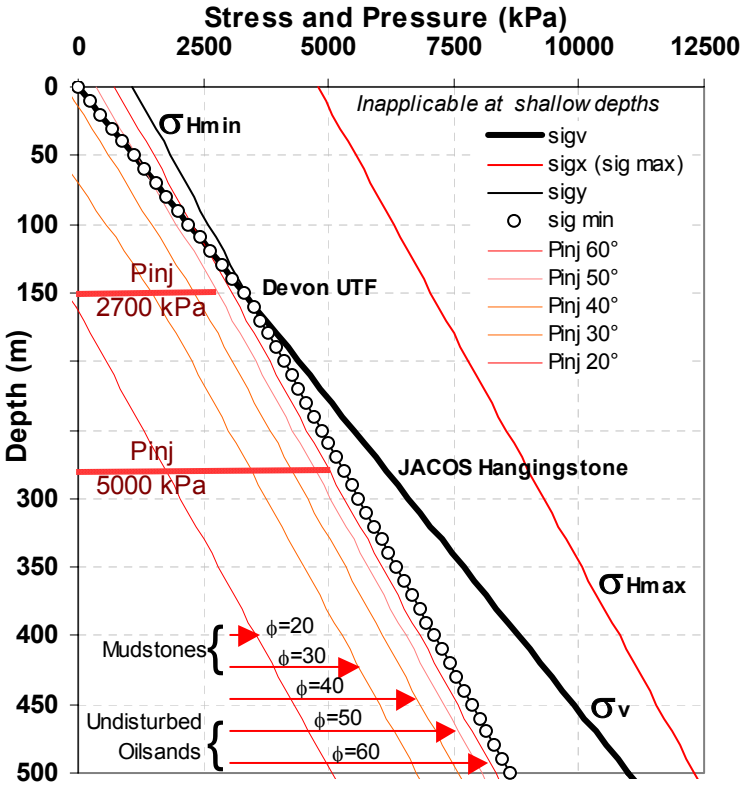

This prediction of P_{inj} is for any injection scheme, thermal or non-thermal. Processes using non-thermal injection schemes below fracture pressures should operate at or above P_{inj} to ensure that the beneficial effects of formation shearing are obtained. Given the performance of the UTF and Hangingstone projects, and the typical strength properties of Athabasca oilsands, a friction angle of 50° would be appropriate for most projects (**Equation 11**). Triaxial tests could be done to determine a site-specific friction angle. However, coring, retrieval, and testing procedures must be

designed to obtain the required undisturbed geomechanical core specimens.

Thermodynamically-driven analyses[16] would indicate economic benefits of operating pure steam injection projects at lower temperatures (and therefore lower pressures). However, these implicitly presume the benefits of geomechanical enhancement by using high permeabilities, independently of operating pressure. It is improbable that such permeabilities will be achieved *in situ* at lower operating pressures.

It may be possible to co-inject steam with another gas to obtain the required high pressures for shearing yet retain thermodynamic efficiency.

A more exacting analysis would include the effects of poroelasticity (**Equations 5 & A14**). This would reduce both horizontal stresses by $\alpha\Delta p\nu/(1-\nu)$, where Δp is the change in reservoir pressure with injection. However, both horizontal stresses would be reduced equally; therefore the net effect on P_{inj} for deeper reservoirs would be zero and Equations 9 to 11 are valid.

Conversely, for shallower reservoirs, the minimum *in situ* stress is the total vertical stress; this remains constant, despite the change in reservoir pressure. Since injection will reduce the stress differential in this case, a slightly higher injection pressure would be required to induce shear failure. However, at shallower depths the predicted horizontal stresses using tectonics are unrealistic (i.e., they have been relieved). Therefore a correct determination of the actual stresses is far more critical than any secondary effects of poroelasticity.

Thermal Effects in the Athabasca Oilsands. For shallow projects, thermal stresses will enhance *in situ* recovery processes. Although there may be some local variation, the minimum *in situ* stress will be the vertical stress, which is limited to the weight of the overburden. As such, vertical thermal stresses are relieved by uplift. However, thermal stresses will increase the horizontal stresses. This combination of effects increases the differential stress, which enhances shearing. If the well were aligned perpendicular to the maximum horizontal stress, this would encourage lateral spreading of the heated volume, e.g.: steam chamber. If aligned at right angles to this, the steam chamber would tend to have a pronounced development along the well axis. Thus,

Figure 6 Radial and Tangential Stresses beyond Steam Chamber

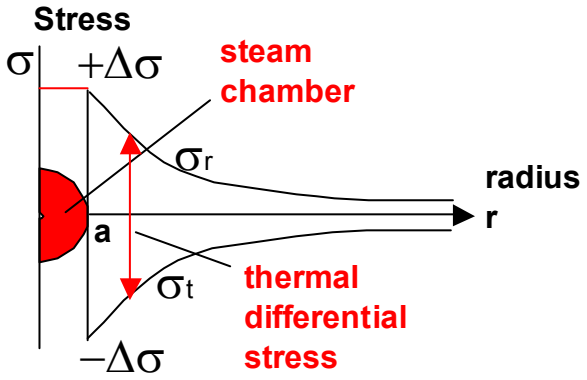

process development is sensitive to well orientation.

For deeper reservoirs, the thermal behaviour is much more complex, and situationally dependent.

Ahead of the steam chamber the thermal expansion of the steam chamber increases the differential stresses by creating positive radial stresses and negative tangential stresses **(Figure 6)**. At the perimeter of the steam chamber, if the radial stress is co-aligned with the maximum *in situ* stress, the thermal stresses will contribute to the maximum stress. Similarly, where the tangential stress is co-aligned with the minimum *in situ* stress, it will further lower that stress. Both these conditions will enhance shearing just outside of the expanding steam chamber, thereby accelerating the steam chamber growth. Although there are orientations around the steam chamber where these stresses tend to lessen the *in situ* stress differential, the overall effect will be positive.

As a first approximation, the heated zone can be idealized as a heated cylinder within an infinite medium. The uniform thermal stress within the cyclinder, which pushes outwards on the colder reservoir, can be calculated using parameters for an analogue reservoir to the UTF project:

P_{inj} = 2700 kPaa T = 228°C (saturated steam)
E = 200 MPa (lower stiffness at lower confining stress)
ν = 0.3
α_T = 4.0E-05 $°C^{-1}$
Δp = (2700-101-550) kPa = 2049 kPa
ΔT = (228-8)°C = 220°C

substituting these into **Equation D10**,

$\Delta\sigma$ =1257+585 = 1842 kPa

The first term, 1257kPa, represents the thermal stress that is greater than the poroelastic component, 585 kPa.

As with **Figure 6**, the cylindrical steam chamber is pushing outwards with 1842 kPa, therefore the radial stresses would increase by 1842 kPa and the tangential stresses decrease by that amount. In reality, there is a temperature gradient outside the steam chamber, so these values would be an upper limit to the incremental stress changes.

As the recovery pattern matures and more of the reservoir becomes heated, other factors begin to affect the stresses in the reservoir. For example, thermal jacking, where the expanding steam chambers around wellpairs unload the vertical stress of the cold oilsands between them, becomes more prominent. This increases deviatoric stresses, which promotes shearing. By this late stage of the SAGD process, shearing and dilation of should be pervasive throughout the reservoir. Once the reservoir is dilated, the associated benefits are irreversible. Towards the end of the process, projects typically operate at reduced temperatures and pressures to obtain the benefits of some thermal recovery from the depleted zones.

Conclusions

A methodology was presented with which the stress tensor for the Athabasca oilsands could be estimated. The method is based on principles from geomechanics and solid mechanics. The resultant stresses are consistent with the geological setting and measured values of vertical and minimum horizontal stresses.

The injection pressure required to ensure shear failure, and its associated benefits to absolute permeability and fluid mobility, were calculated assuming a Mohr-Coulomb failure criterion for the oilsands. A friction angle of 50° was found to reasonably predict observed behaviour in Athabasca oilsands. From this, the geomechanically optimal injection pressure was determined, as a function of depth. This pressure is recommended for in situ injection schemes, both thermal and non-thermal.

Thermal effects were generally found to enhance the recovery scheme, particularly during the initial period of injection. Dilation and enhanced permeabilities obtained during early steaming would be permanent and irreversible.

From a geomechanics perspective, injection pressures should remain high enough to maximize shearing and dilation throughout the reservoir.

Acknowledgements

The author would like to thank Newmont Mining Corporation of Canada Limited for permission to present these data, and to Applied Reservoir Engineering Limited for their support.

Nomenclature

a = radius of the cylinder
B = Skempton's pore pressure coefficient
CGR = corrected gamma ray (API)
d = distance from the neutral axis (m)
E = Young's modulus (MPa)
G = shear modulus (MPa)
K = bulk modulus (drained) (MPa)
K'_s = bulk modulus of the grains
K_f = bulk modulus of the pore fluid
K_u = bulk modulus (undrained)
K_ϕ = unjacketed pore bulk modulus: the change in pore pressure per unit pore volume change, when the confining stress equals the pore pressure
k = curvature = radius^{-1} (m^{-1})
kPaa = kPa absolute
P_{inj} = injection pressure
p_f = formation fluid pressure
SAGD = steam-assisted gravity drainage
T = temperature
ΔT = change from the original formation temperature
u_T = thermal radial expansion of the cylinder
z = is the vertical depth (metres)

α = Biot-Willis pore pressure coefficient
α_T = coefficient of thermal expansion ($°C^{-1}$)
ε_x , ε_y , ε_z = principal strains in the x,y,z orientations
ϕ porosity
$\phi°$ friction angle
σ = total stress
σ' = effective stress
σ_h = horizontal stress (i.e., fracture gradient)
σ_{Hmax} , σ_H = maximum horizontal stress
σ_{Hmin} , σ_h. = minimum horizontal stress
σ_{max} = maximum *in situ* stress
σ_{min} = is the minimum *in situ* stress
σ_r = radial stress
σ_t = tangential stress
σ_v = vertical stress
σ_x = stress in the x-direction
σ_y = stress in the y-direction
σ_x , σ_y , σ_z = stresses in the principal x,y,z orientations
σ_3 = $_{confining}$ stress, or minimum principal stress
σ'_3 = effective confining stress
$\Delta\sigma$ = change in stress
$\Delta\sigma_{kk}$ = change in octahedral stress (=$\Delta\sigma_x$+$\Delta\sigma_y$+$\Delta\sigma_z$)
$\Delta\sigma_x$, $\Delta\sigma_y$, $\Delta\sigma_z$ = change in stress in the principal x,y,z orientations
$\Delta\sigma_T$ = change in stress due to thermal effects
ν = Poisson's ratio
$\sim$ = "*approximately*"

References

1) Timoshenko, S.P., and Goodier, J.N. (1934) *Theory of Elasticity*, publ. McGraw-Hill Inc., 567pp.
2) Terzaghi, K. (1943) *Theoretical Soil Mechanics*, publ. John Wiley and Sons, Inc., 510pp.
3) Wang, H.F. (2000) "Theory of Linear Poroelasticity with Applications to Geomechanics and Hydrogeology", publ. Princeton University Press, Princeton, N.J. U.S.A., 287pp.
4) Eaton, B.A. (1969) "Fracture Gradient Prediction and Its Application in Oilfield Operations", SPE2163, *JPT* **21**, pp.1353-1360
5) Guenot, A. (1989) "Borehole Breakouts and Stress Fields", *Int. J. Rock Mech. Min. Sci. & Geomech. Abstr.*, **V26,** No. 3/4, publ. Pergamon Press Plc., U.K. pp.185-195.
6) Cox, J.W. (1983) "Long axis orientation in elongated boreholes and its correlation with rock stress data":, proc. SPWLA Twenty-Fourth Ann. Logging Symp., June 27-30, 17pp.
7) Mueller, B., Reinecker, J., Heidbach, O. and Fuchs, K. (2000): *The 2000 release of the World Stress Map,* publ. online http://www.world-stress-map.org, Heidelberg Academy of Sciences and Humanities, Institute of Geophysics, Karlsruhe University
8) Hepler L.G. and C. His (eds.) **AOSTRA Technical Handbook on Oil Sands, Bitumens and Heavy Oils**, (1989) publ. Alberta Oil Sands Technology and Research Authority, Edmonton, Alberta, 376pp.
9) Chalaturnyk, R.J. (1996) **Geomechanics of the steam assisted gravity drainage process in heavy oil reservoirs**, Ph.D. thesis, Dept. of Civil Eng., U. of Alberta, Edmonton, Alberta 576 pp.
10) Hannan, S.S., and B.I. Nzekwu (1992) **AOSTRA Mini-Frac manual - Field Testing, Analysis and Interpretation Procedures**, AOSTRA Tech. Publ. Series No. 13, publ. Alberta

Oil Sands Technology and Research Authority, Edmonton, Alberta, 78pp.
11) Ito, Y., M. Ichikawa, and T. Hirata (2000) "The growth of the steam chamber during the early period of the UTF Phase B and Hangingstone Phase I projects", paper 2000-05, Pet. Soc. of CIM Can. Int. Pet. Conf., June 4-8, Calgary, Alberta, 16pp.
12) Kry, P.R. (1989) "Field observations of steam distribution during injection to the Cold Lake Reservoir", proc Rock at Great Depth: Rock mechanics and rock physics at great depth,. ISRM-SPE Int. Symp., Pau, France, Oct. 28-31, pp.853-861.
13) Touhidi-Baghini, A. (1998) **Absolute permeability of McMurray Formation oil sands at low confining stresses**, Ph.D. thesis, Dept. of Civil Eng., U. of Alberta, Edmonton, Alberta 339 pp.
14) Touhidi-Baghini, A. and J.D. Scott (1998) "Absolute permeability changes of oil sand during shear", proc. 51st Can. Geotechnical Conf., Edmonton, Alberta, pp.729-736.
15) Dusseault, M.B. (1980) "Sample disturbance in Athabasca oil sand", *JCPT*, April-June, pp.85-92.
16) Edmunds, N.R. and H. Chhina (2001) "Economic Optimum Operating Pressures for SAGD Projects in Alberta" Dist. Auth. Series, *JCPT, Dec.*
17) Craig, R.F. (1978) "Soil Mechanics", 2nd ed., publ. Van Nostrand Reinhold Co., Toronto, 318pp.
18) personal communication, Dr. R.J. Chalaturnyk, P.Eng., Dept of Civil and Environmental Engineering, University of Alberta, Edmonton, Alberta.
19) Jaeger, J.C. and Cook, N.G.W. (1976) *Fundamentals of Rock Mechanics,* 2nd ed., publ. Chapman and Hall, London, 585pp.
20) Gretener, P.E. (1969) "On the Mechanics of the Intrusion of Sills", *Can. J. E. Sc.*, 6/6 pg.1415-1419
21) Blanton, T.L., and Olson, J.E. (1997) "Stress Magnitudes From Logs: Effects of Tectonic Strains and Temperature", SPE38719, proc., 1997 ATCE of SPE, San Antonio, TX, USA, 5-8 October 1997, 12pp.
22) Ericsson, Julia B., McKean, Howard C., and Hooper, Robert J. (1996) "Interdependence of fractures, facies, and fluid flow in a Late Cretaceous Arabian Gulf carbonate", presentation by Ericsson at the *Faulting, Fault Sealing and Fluid Flow in Hydrocarbon Reservoirs Conference*, U. of Leeds, Leeds, U.K., 23-25 Sept. 1996, abstract only.
23) accreditted to John Graham, P.Eng., Thurber Engineering Ltd., Edmonton, Alberta.

Metric Conversion Factors

1 ft = 0.3048 metre
1 psi = 6.8947 kPa
1 psi/ft = 22.62 kPa/m
1 SG = 1.00 g/cm^3
= 8.34543 ppg
°F = (°C*1.8)+32

Appendix A

Fluid Pressure Effects. An increase in fluid pressure will reduce effective stresses. In Eaton's equation, the effective stress term (σ_v-p_f) is factored by $\upsilon/(1-\upsilon)$, therefore the net effect of a pressure increase will be an increase in total stress.

To examine the interaction between external stress and internal fluid pressure, consider the case of an element of rock with fluids in its pore space. The stresses in the rock and the fluid pressure are in equilibrium with the external stresses. This element of rock is then subjected to an increase in total stress in all directions, $\Delta\sigma_3$ under undrained conditions, i.e. no fluids enter or leave the element. If the individual rock grains are considered incompressible in comparison to the rock matrix or the fluids, the pressure response to a change in an external isotropic stress is described by the Biot parameter for pressure[17], or Skempton's coefficient B:

$$\Delta p_f = B\Delta\sigma_3 \quad \text{.....[A1]}$$

$$\text{where } B = \frac{1}{1+\phi\left(\frac{C_v}{C_s}\right)} \quad \text{.....[A2]}$$

B Biot pore pressure coefficient
C_s compressibility of the rock matrix under the application of an isotropic effective stress change (not the individual grain compressibility)
C_v compressibility of the pore fluid under an isotropic pressure increment
ϕ porosity
$\Delta\sigma_h$ change in horizontal stress
$\Delta\sigma_3$ change in confining stress (isotropic)

The increase in pore pressure is less than the applied stress because of the compressibilities of the rock matrix and the pore fluids. For compressible rock matrices and fluid-filled pores, $B\rightarrow 1$ since the pore fluid will support the added load. For gas-filled pores, $B\rightarrow 0$ since the matrix must support the load. For the Athabasca oil sands, the Biot parameter for an undisturbed specimen[5] would be $B\approx 0.75$, requiring that the undisturbed rock matrix and pore liquid compressibilities be comparable. This means that any application of an external isotropic load will result in the pore fluids taking 75% of that increase, and the rock matrix taking 25%. Higher values of B are indicative of higher rock matrix compressibilities and, therefore, of sample disturbance[18].

This Biot parameter is only applicable for undrained conditions. In its determination, the element of rock is also free to deform in response to the isotropic applied total stress, $\Delta\sigma_3$.

The scenario of an increase in formation fluid pressure, Δp_f, as would occur when injecting into the reservoir, requires the superposition of the outward expansion of the element, and the re-imposition of zero lateral strains. will result in an increase in the pore volume by $C_v\phi\Delta p_f$, with an identical increase in the rock matrix volume. This changes the total stresses by the amount:

$$\Delta\sigma_3 = \Delta p_f / B = \Delta p_f + \Delta p_f \phi\left(\frac{C_v}{C_s}\right) \quad \text{.....[A3]}$$

The external total stress increase , $\Delta\sigma_3$, is slightly greater than the applied internal fluid pressure change, Δp_f , due to the rock matrix expanding outwards as the pore volume increases.

Since the applied condition is the full increase in formation fluid pressure, Δp_f, the isotropic *effective* stress change is:

$$\Delta\sigma_3' = \Delta p_f \phi\left(\frac{C_v}{C_s}\right) \quad \text{[A4]}$$

However, the total vertical stress is limited by the overburden stress, therefore the formation would displace vertically. In the horizontal plane, the formation is constrained, therefore the changes in the three principal stresses are:

$$\Delta\sigma_h = \frac{\upsilon}{1-\upsilon}\left(-B\Delta p_f\right) + B\Delta p_f \quad \text{[A5]}$$

$$\Delta\sigma_y = \Delta\sigma_x \quad \text{[A6]}$$

$$\Delta\sigma_z' = 0 \quad \text{[A7]}$$

where

B is the Biot pore pressure coefficient

C_s is the compressibility of the rock matrix under the application of an isotropic effective stress change

C_v is the compressibility of the pore fluid under an isotropic pressure increment

ϕ is the porosity

$\Delta\sigma_h$ is the change in horizontal stress

$\Delta\sigma_3$ is the change in confining stress (isotropic)

For the specific boundary conditions of zero lateral strain and a constant vertical stress, allowing drainage[3]:

$$\varepsilon_x = \frac{1}{2G}\left(\Delta\sigma_x - \frac{\upsilon}{1-\upsilon}\Delta\sigma_{kk}\right) + \frac{\alpha}{3K}\Delta p_f \quad \text{[A8]}$$

$$\varepsilon_y = \frac{1}{2G}\left(\Delta\sigma_y - \frac{\upsilon}{1-\upsilon}\Delta\sigma_{kk}\right) + \frac{\alpha}{3K}\Delta p_f \quad \text{[A9]}$$

$$\varepsilon_z = \frac{1}{2G}\left(\Delta\sigma_z - \frac{\upsilon}{1-\upsilon}\Delta\sigma_{kk}\right) + \frac{\alpha}{3K}\Delta p_f \quad \text{[A10]}$$

$$\Delta\sigma_y = \Delta\sigma_x \quad \text{[A11]}$$

$$\Delta\sigma_z' = 0 \quad \text{[A12]}$$

where

G is the shear modulus

K is the bulk modulus

ϕ is the porosity

ε_x, ε_y, ε_z are the principal strains in the x,y,z orientations

$\Delta\sigma_x$, $\Delta\sigma_y$, $\Delta\sigma_z$ are the changes in principal total stresses

$\Delta\sigma_{kk}$ is the change in octahedral stress ($=\Delta\sigma_x+\Delta\sigma_y+\Delta\sigma_z$)

Figure A1 Oedometric Boundary Conditions with Constant Vertical Stress

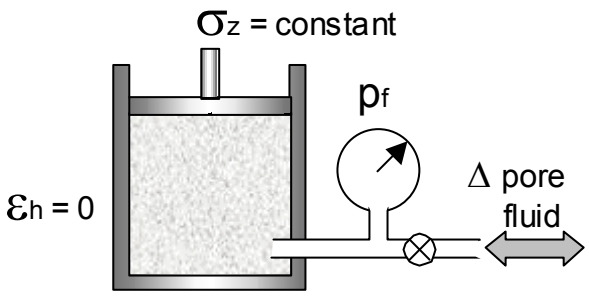

When the conditions of lateral constraint with constant vertical stress are applied (**Figure A1**) the change in total horizontal stress ($\Delta\sigma_x=\Delta\sigma_y=\Delta\sigma_h$) due to a change in pore pressure only, due to fluid injection or production is:

$$\Delta\sigma_h = \frac{1-2\upsilon}{1-\upsilon}\alpha\Delta p_f \quad \text{[A13]}$$

This is a total stress change, which includes the pore pressure change. The change in effective stress is the total stress minus the factored pore pressure:

$$\Delta\sigma_h' = \Delta\sigma_h - \alpha\Delta p_f = \frac{-\upsilon}{1-\upsilon}\alpha\Delta p_f \quad \text{[A14]}$$

Although the total vertical stress remains constant, the effective vertical stress does drop by αp_f. The Poisson's effect causes this reduction in effective horizontal stress in response to the reduction in the vertical effective stress.

Pore Pressure Coefficients α and B. The two pore pressure coefficients differ. The Biot-Willis coefficient "α" is a function of the stiffness of the rock matrix relative to the stiffness of the constituent rock particles (solids), measured under drained conditions. The Skempton coefficient "B" is a function of the compressibility of the pore fluid relative to the rock matrix, under undrained conditions.

Coefficient "B" can also be defined as:

$$B = \frac{1/K - 1/K_s'}{1/K - 1/K_s' + \phi(1/K_f - 1/K_\varphi)} \quad \text{[A15]}$$

$$B = \frac{1 - K/K_u}{1 - K/K_s'} \quad \text{[A16]}$$

where

K is the bulk modulus (drained)

K'_s is the bulk modulus of the grains

K_f is the fluid modulus

K_u is the bulk modulus (undrained)

K_ϕ is the unjacketed pore bulk modulus: the change in pore pressure per unit pore volume change, when the confining stress equals the pore pressure

ϕ is the porosity

Coefficient B tends towards zero when gas fills the pore space, and tends towards one when liquids fill the pore space.

Appendix B

Tectonic Effects. In its simplest manifestation, tectonics applies a uniform lateral strain through the rock strata. This can either be a positive (compressive) strain, as in the case of orogenic thrust, or negative (tensile) strain, as in the case of lateral spreading of compacting sediments. For the case of a horizontal rock stratum experiencing a compressive uniaxial strain only in the "x" direction, the conditions are:

$$\varepsilon_x \Rightarrow increases \quad \text{[B1]}$$

$$\Delta\varepsilon_y = 0 \quad \text{[B2]}$$

$$\Delta\sigma_z = 0 \quad \text{[B3]}$$

Unless this strain is relieved, as might occur as a result of faulting, the horizontal stress increases in the rock[19], in the direction of straining:

$$\Delta\sigma_x = \frac{E}{(1-\nu^2)}\varepsilon_x \quad \text{[B4]}$$

Significantly, the stress in the perpendicular horizontal direction also increases, due to ε_x and the Poisson's effect, but to a lesser extent:

$$\Delta\sigma_y = \frac{\nu E}{(1-\nu^2)}\varepsilon_x \quad \text{[B5]}$$

Figure B1 Uniaxial Horizontal Strain

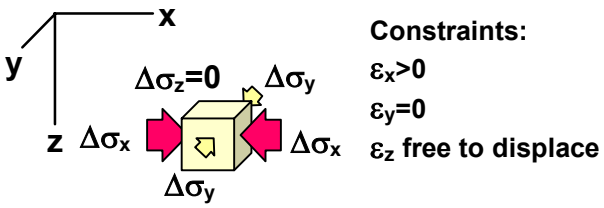

Note that in a region of compressive strain, the minimum horizontal stress, σ_{Hmin}, will be in the "y" orientation, whereas in a region of tensile strain, σ_{Hmin} will be in the "x" direction.

The vertical stress remains unchanged: any Poisson's effect in the vertical direction is relieved by an upward displacement of all rock strata. This vertical strain, due to a uniform horizontal strain in the "x" direction, is:

$$\varepsilon_z = \frac{-\nu}{1-\nu}\varepsilon_x \quad \text{[B6]}$$

The implications of these equations are significant. First, stresses in areas that have experienced straining, such as from tectonics, will have horizontal stresses that can be very different than those predicted with Eaton's equation, which assumes zero lateral strain. Next, the increases in stress will

Figure B2 Tectonic Strains and Stresses

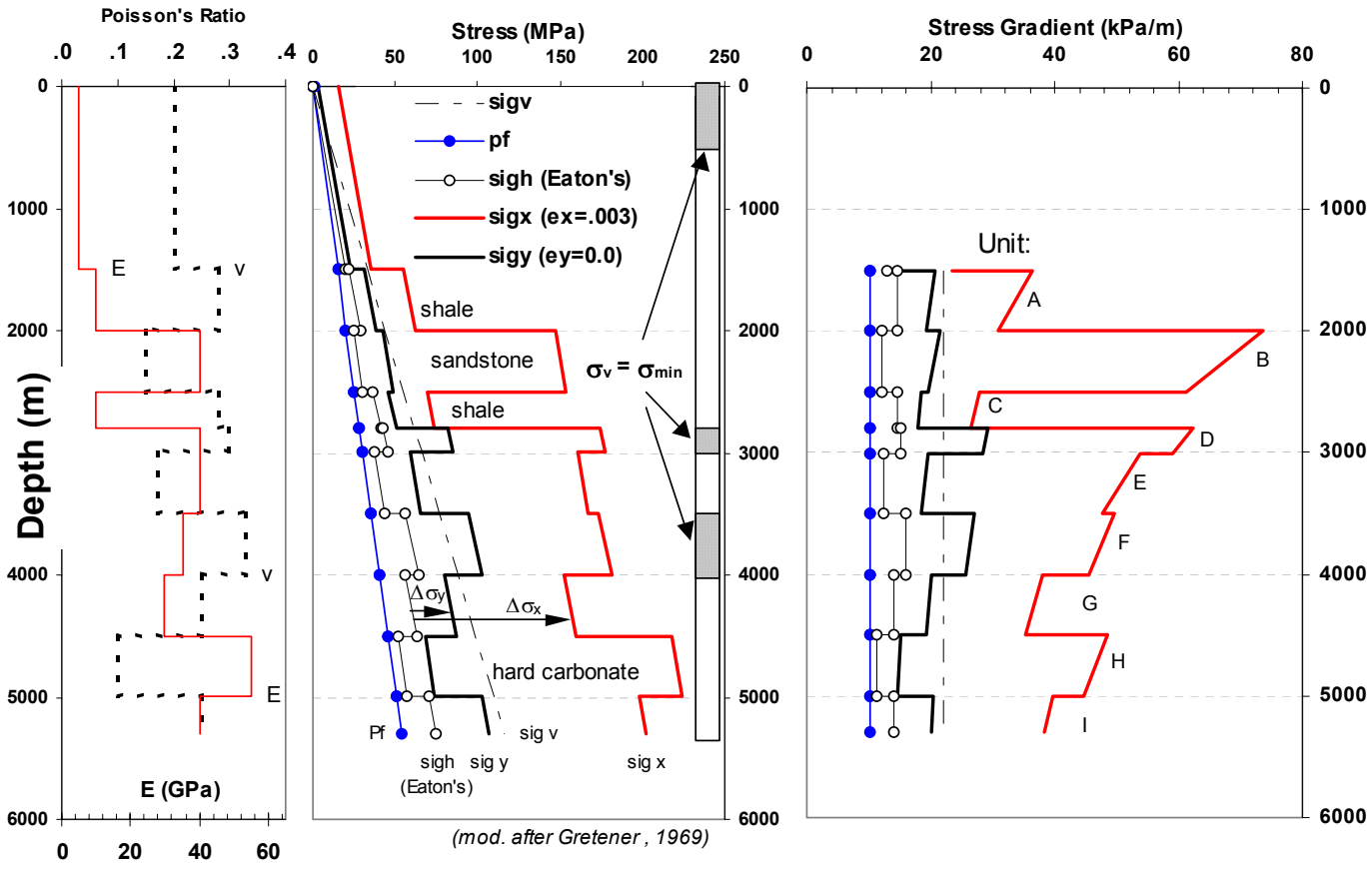

vary from formation to formation, largely in proportion to their respective Young's moduli, with the stiffer strata being much more affected by strain. Lastly, the stress in the direction transverse to the tectonic strain will also change. In a compressive tectonic regime, the transverse horizontal stress will be the minimum *in situ* stress until such time as the tectonic straining increases both horizontal stresses above the vertical stress. The applications of these principals to hydraulic fracture stimulation are obvious in terms of determining the direction of fracture propagation, the increase in fracture closure stress, the orientation of the induced hydraulic fracture, and fracture containment.

Figure B2 shows three graphs: an arbitrary profile of E and ν, stress and pressure profiles, and stress gradient profiles. In the middle graph, the pore pressure gradient is a constant 1.03 S.G. (10.1 kPa/m), and the vertical stress gradient is 22 kPa/m. These are shown as the straight lines labelled "pf" and "sigv", respectively. The value of the uniform horizontal stress, "sigh", has been calculated using Eaton's equation, which assumes zero lateral strain. This line appears as a series of line segments due to the variation in the value of Poisson's ratio between each stratigraphic unit.

Next, a uniform lateral strain of 0.3% was applied in the "x" horizontal direction[20,21]. No strain was allowed in the "y" horizontal direction. In response to this strain, the horizontal stresses have increased significantly. The largest increase is in the horizontal stress in the x-direction, σ_x, and a smaller increase is seen in the horizontal stress in the y-direction, σ_y, due to the Poisson's effect. The pore pressure and vertical stress remain unchanged.

The largest increases in σ_x occur in the stiffest rock, as would be expected from Equation B4. The increase in σ_y is a proportion of that, being factored by the Poisson's ratio (**Equation B5**). Notably, σ_y is far greater than the horizontal stress predicted by assuming zero lateral strain.

Three zones: the near-surface, Unit D and Unit F, have undergone horizontal stress increases to the extent that the vertical stress is the minimum *in situ* stress. This is a credible outcome, and is the required condition for overthrust faulting to occur: the rock displaces in the direction of least resistance, i.e. vertically. Any induced hydraulic fractures in these intervals would propagate horizontally. The horizontal stresses near surface are partially relieved by folding, faulting, or shearing along weaker strata, producing displacement features such as slickensides.

Unit B is a sandstone sandwiched between shale units. Without tectonic strains, the minimum *in situ* stress is the uniform horizontal stress. Very small tectonic strains would result in horizontal stress anisotropy, which would control the orientation of any induced hydraulic fracture, but the fracture would still be vertically constrained by the higher stresses in the bounding shales. However, after the tectonic strain has increased to 0.3%, the minimum horizontal stress ($\sigma_{Hmin} = \sigma_y$) has increased such that it exceeds σ_{Hmin} in the bounding shales. This occurs because the shales have a lower stiffness and therefore the tectonic stress increase is smaller for the same strain. Containment of any induced hydraulic fracture is uncertain, since any fracture breakthrough into either bounding shale would result in the fracture propagating into the shales.

Bidirectional Strains. In more complex environments, it is possible to have strains in both principal horizontal strain directions. The generalized equations for stress and strain due to tectonic strains in both the "x" and "y" horizontal orientations are:

$$\Delta\sigma_x = \frac{E}{(1-\nu^2)}\varepsilon_x + \frac{\nu E}{(1-\nu^2)}\varepsilon_y \quad \text{[B7]}$$

$$\Delta\sigma_y = \frac{\nu E}{(1-\nu^2)}\varepsilon_x + \frac{E}{(1-\nu^2)}\varepsilon_y \quad \text{[B8]}$$

$$\Delta\sigma_z = 0 \quad \text{[B9]}$$

$$\varepsilon_z = \frac{-\nu}{1-\nu}\varepsilon_x + \frac{-\nu}{1-\nu}\varepsilon_y \quad \text{[B10]}$$

Appendix C

Post-Depositional Curvature Effects. Mechanisms such as tectonic compression, halokinetics, and intrusion into substrata can result in rock bending or "folding" (**Figure C1**). Incompetent strata, such as shales, will flow plastically or shear in a geological timeframe. Folding results in flexural stresses within the competent strata. Flexural stresses are usually incidental to the Athabasca oilsands since post-depositional deformation has not generally occurred. The exception is when there are deformations due to isolated and localized salt dissolution below the carbonate underburden.

Figure C1 Schematic of Similar Folding

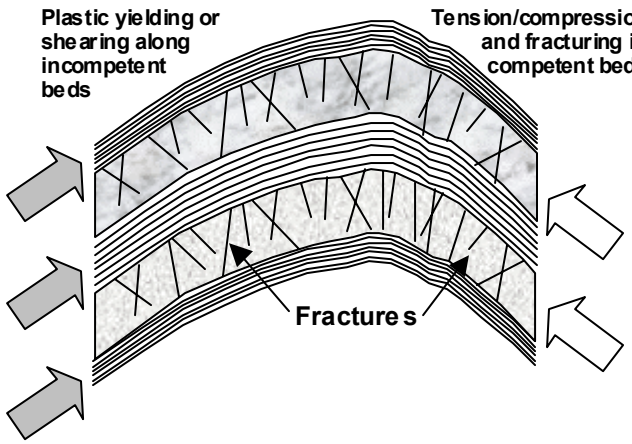

Competent strata, such as sandstones and carbonates, develop localized strains that vary with the degree of bed curvature, and the location within each stratum. In similar folding, in which strata have identical radii of curvature, the incompetent beds act to isolate the flexural behaviour of each competent bed. In concentric (parallel) folding, the strata can be considered as a composite beam.

The flexural stresses and strains are tensile on the convex side and compressive on the concave side, and are calculated using classical beam theory. Net vertical strains are approximately zero since the positive and negative strains resulting from the compressive and tensile stresses within each stratum will cancel each other out. The flexural stresses resulting from bending vary with the distance from the neutral axis, in this case, the centre of the competent bed:

$$\Delta\sigma_x = k_x \cdot E \cdot d \quad \text{[C1]}$$

where

$\Delta\sigma_x$ is the change in horizontal stress in the x direction
k_x is the local curvature in the x-z plane
E is Young's Modulus
d is the distance from the neutral axis, e.g.: the middle of each bed for similar folds

The curvature "k" is the inverse of the radius of the post-depositional deformation, which is usually several kilometres, and excludes any syndepositional curvature. The flexural stresses can be generalized for the case of biaxial bending:

$$\Delta\sigma_x = k_x \cdot E \cdot d + \nu\left(k_y \cdot E \cdot d\right) \quad \text{[C2]}$$

$$\Delta\sigma_y = \nu\left(k_x \cdot E \cdot d\right) + k_y \cdot E \cdot d \quad \text{[C3]}$$

$$\varepsilon_z \cong 0 \quad \text{[C4]}$$

Net vertical strains are approximately zero since the positive and negative strains resulting from the compressive and tensile stresses within each stratum will cancel each other out.

Fracture gradients will vary within each stratum as a function of the degree of curvature, the stiffness of the stratum, the thickness of the stratum, and the location with it. Folded stiff beds, such as those within carbonate reservoirs in the Middle East, and can have significantly lower fracture gradients at the crest of the structure, where the curvature is often greatest, than at the shoulders. Similarly, the tops of each bed will have lower fracture gradients than the bottoms.

Ericsson, et al. (1996)[21] noted that the crest of their structure had more open fractures than elsewhere. The high-curvature grainstones and packstones had 82% of their fractures. Aramco was also noted to use curvature of the formations in their planning.

Appendix D

Thermal Effects. Rock will try to expand when subjected to a change in temperature. Under laterally constrained conditions, the resistance to thermal expansion due to a uniform temperature change will create a horizontal thermal stress in the rock:

$$\Delta\sigma_T = \frac{E}{1-\nu}\alpha_T \Delta T \quad \text{[D1]}$$

where

$\Delta\sigma_T$ is the change in stress due to thermal effects
α_T is the coefficient of thermal expansion
E is Young's modulus
ν is Poisson's ratio
ΔT is the change from the original formation temperature

Localized effects are more complex. The initial heating of a well will create an annulus of heated rock that expands with time. For the case of horizontal wells and the SAGD process, the heated zone consists of the steam chamber, with a proximal falloff of temperatures outside the steam chamber.

Figure D1 Schematic Idealization of Steam Chamber

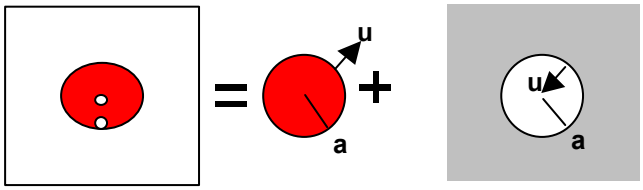

As a first order approximation, the steam chamber can be idealized as a perfect cylinder within an infinite medium, assuming plane strain boundary conditions (**Figure D1**). This in turn can be considered as two separate problems: a heated cylinder, and a hole in an infinite medium. The solutions for each can be linked by equating the displacements on the surface of the cylinder with the hole surface[23].

The displacement on the outside of the uniformly heated cylinder are[1]:

$$u_T = a(1+\upsilon)\alpha_T \Delta T \quad \text{[D2]}$$

where

u_T is the thermal radial expansion of the cylinder
α_T is the coefficient of thermal expansion
a is the radius of the cylinder
ν is Poisson's ratio
ΔT is the change in temperature

Adding poroelasticity effects, this becomes:

$$u = a(1+\upsilon)\alpha_T \Delta T + \frac{\Delta p_f (1-2\upsilon)(1+\upsilon)}{E} a \quad \text{[D3]}$$

Any hydrostatic stress, $\Delta\sigma$, acting on the cylinder surface will cause a contraction:

$$u_\sigma = \frac{\Delta\sigma(1-2\upsilon)(1+\upsilon)}{E} a \quad \text{[D4]}$$

The identical stress, $\Delta\sigma$, acting on the hole surface within the infinite medium will increase its radius by:

$$u_{hole} = \frac{\Delta\sigma(1+\upsilon)}{E} a = u_\sigma (1-2\upsilon) \quad \text{[D5]}$$

The thermal expansion of the cylinder, minus the contraction due to the confining (hydrostatic) stress, must equal the displacement of the hole at that same stress:

$$u_T - u_\sigma = u_{hole} \quad \text{[D6]}$$

$$u_T = u_{hole} + u_\sigma \quad \text{[D7]}$$

$$u_T = 2(1+\upsilon)u_\sigma \quad \text{[D8]}$$

Solving for the interfacial stress:

$$\Delta\sigma = \frac{E}{2(1-\upsilon)(1+\upsilon)a} u_T \quad \text{[D9]}$$

$$\Delta\sigma = \frac{E\alpha_T \Delta T}{2(1-\upsilon)} + \frac{\Delta p_f (1-2\upsilon)}{2(1-\upsilon)} \quad \text{[D10]}$$

This represents a uniform stress within the cylindrical steam chamber, and is independent of its radius. However, for the surrounding infinite medium, this is also the hydrostatic stress at the interface with the steam chamber. As such, the incremental radial and tangential stresses will vary within the medium with distance from the steam chamber (**Figure 6**):

$$\sigma_r = +\Delta\sigma \frac{a^2}{r^2} \quad \text{[D11]}$$

$$\sigma_t = -\Delta\sigma \frac{a^2}{r^2} \quad \text{[D12]}$$

$$\tau_{rt} = 0 \quad \text{[D13]}$$

At the perimeter of the steam chamber, where the radial stress is co-aligned with the maximum *in situ* stress, the thermal stresses will contribute to maximum stress. Similarly, where the tangential stress is co-aligned with the minimum *in situ* stress, it will further lower that stress. Both these conditions will enhance shearing outside of the steam chamber. Conversely, at orientations around the steam chamber where these stresses tend to lessen the *in situ* stress differential, shearing will be inhibitted.

Further refinements of this methodology can be made to account for the fact that the near-wellbore heated region is similar to a thick-walled cylinder, with an initial gap between the sandface and the screens. While the shearing and dilation of the sandface have implications for near wellbore skin factors, they are not relevant to the determination of injection pressures.

Appendix E

Other Effects. In addition to those mechanisms discussed here, other factors can increase or decrease stresses in the rock: mineral alteration (particularly those that result in volumetric change), chemical or pressure dissolution, bed elongation as strata compact and consolidate in depositional basins, nearby intrusives (mud or salt diapirism), and complex geological structures. Their stress effects should be included, where appropriate. This can often be done with the superposition of elastic solutions onto the existing stress regime, as was done for the thermal effects.